Published in final edited form as:
Neuroimage. 2008 October 1; 42(4): 1451–1462. doi:10.1016/j.neuroimage.2008.05.066.

A Tractography Comparison between Turboprop and Spin-Echo Echo-Planar Diffusion Tensor Imaging

Minzhi Gui[1], **Huiling Peng**[1], **John D. Carew**[2], **Maciej S. Lesniak**[3], and **Konstantinos Arfanakis**[1,4]

1*Department of Biomedical Engineering, Illinois Institute of Technology, Chicago, IL*

2*Departments of Biostatistics and Radiology, Emory University, Atlanta, GA*

3*Department of Surgery, The University of Chicago, Chicago, IL*

4*Brain Research Imaging Center, The University of Chicago, Chicago, IL*

Abstract

The development of accurate, non-invasive methods for mapping white matter fiber-tracts is of critical importance. However, fiber-tracking is typically performed on diffusion tensor imaging (DTI) data obtained with echo-planar-based imaging techniques (EPI), which suffer from susceptibility-related image artifacts, and image warping due to eddy-currents. Thus, a number of white matter fiber-bundles mapped using EPI-based DTI data are distorted and/or terminated early. This severely limits the clinical potential of fiber-tracking. In contrast, Turboprop-MRI provides images with significantly fewer susceptibility and eddy-current-related artifacts than EPI. The purpose of this work was to compare fiber-tracking results obtained from DTI data acquired with Turboprop-DTI and EPI-based DTI. It was shown that, in brain regions near magnetic field inhomogeneities, white matter fiber-bundles obtained with EPI-based DTI were distorted and/or partially detected, when magnetic susceptibility-induced distortions were not corrected. After correction, residual distortions were still present and several fiber-tracts remained partially detected. In contrast, when using Turboprop-DTI data, all traced fiber-tracts were in agreement with known anatomy. The inter-session reproducibility of tractography results was higher for Turboprop than EPI-based DTI data in regions near field inhomogeneities. Thus, Turboprop may be a more appropriate DTI data acquisition technique for tracing white matter fibers near regions with significant magnetic susceptibility differences, as well as in longitudinal studies of such fibers. However, the intra-session reproducibility of tractography results was higher for EPI-based than Turboprop DTI data. Thus, EPI-based DTI may be more advantageous for tracing fibers minimally affected by field inhomogeneities.

Keywords

Tractography; DTI; PROPELLER; Turboprop; MRI; Susceptibility

Address Correspondence to: Konstantinos Arfanakis, Ph.D., Department of Biomedical Engineering, Illinois Institute of Technology, 10 West 32nd Street, E1-116, Chicago, IL 60616, e-mail: arfanakis@iit.edu, phone: (312) 567-3864, fax: (312) 567-5707.

Introduction

Estimates of white matter fiber orientation obtained with diffusion tensor imaging (DTI) (Basser *et al.*, 1994, 1995; Pierpaoli *et al.*, 1996) can be used to construct paths that connect different brain regions and are interpreted as representations of the underlying white matter fiber system. This technique is called tractography (Basser *et al.*, 2000) and is currently the only non-invasive method that can provide estimates of brain structural connectivity. Fiber-tractography has been used in studies of white matter structure and brain function (Toosy *et al.*, 2004; Guye *et al.*, 2003), and is gradually becoming an important tool for clinical applications such as pre-surgical planning. More specifically, fiber-tracking has been used to map the cortico-spinal tract, subcortical pathways serving cortical language sites, and the superior longitudinal fasciculus, in patients with brain tumors or other space occupying lesions located in the vicinity of these fiber-tracts (Berman *et al.*, 2004; Clark *et al.*, 2003; Henry *et al.*, 2004). In all cases, knowledge of the exact location of the lesion with respect to eloquent white matter pathways was of great value to the neurosurgeons in planning the appropriate surgical strategy.

The process of mapping white matter fibers is completed in two steps. The first step involves the acquisition of DTI data, and the second the extraction of fiber orientation information from the DTI data and production of white matter connectivity estimates. Several different tractography algorithms have been proposed for the latter. In general, these algorithms can be divided into those that define a single path of connection for each voxel being investigated, (Basser *et al.*, 2000; Le Bihan *et al.*, 2001; Conturo *et al.*, 1999; Jones *et al.*, 1999; Poupon *et al.*, 2000; Stieltjes *et al.*, 2001; Tench *et al.*, 2002; Mori *et al.*, 1999, 2002; Lori *et al.*, 2002; Lazar *et al.*, 2003) and those that produce maps of the probability of connectivity between brain regions (Koch *et al.*, 2002; Behrens *et al.*, 2003; Parker *et al.*, 2003; Jones *et al.*, 2005). However, independent of the tractography algorithm used, the accuracy and reproducibility of fiber-tracking results depend heavily on the noise level and amount of artifacts of the DTI data.

Conventional tractography is performed based on DTI data acquired using spin-echo sequences with diffusion-weighting (DW) gradients and echo-planar signal readout (SE-EPI-DTI) (Lazar *et al.*, 2003). However, these acquisitions suffer from image distortions, signal loss and signal hyperintensities, near regions with magnetic susceptibility differences, such as those at tissue-air and tissue-bone interfaces (Zeng *et al.*, 2002). Furthermore, in DTI when a strong DW gradient is turned on or off, significant eddy currents are induced in conductive parts of the magnet bore and its surroundings, causing geometric distortions in the DW images (Alexander *et al.*, 1997). These geometric distortions produce misalignments between the individual DW images of the DTI dataset, which eventually lead to artifacts in the estimated diffusion tensors. In contrast, PROPELLER imaging (Periodically Rotated Overlapping ParallEL Lines with Enhanced Reconstruction) is an MRI data acquisition and reconstruction technique with greatly reduced sensitivity to various sources of image artifacts (Pipe *et al.*, 1999, 2002). PROPELLER acquisitions follow a multiple-shot fast spin-echo (FSE) approach in which several k-space lines are acquired in each excitation, forming a blade that is then rotated around its center and acquisition is repeated to cover k-space (Pipe *et al.*, 1999, 2002). Since PROPELLER MRI is based on FSE techniques, the images produced contain significantly fewer B_0-related artifacts than those in EPI, and are immune to image warping due to eddy currents (Pipe *et al.*, 2002). Also, in each blade, a central disc of k-space is acquired that can be used as a 2D navigator to correct data between shots without requiring additional echoes (Butts *et al.*, 1996). Comparison of this central k-space disc between blades allows correction of the subject's rotation and translation, as well as identification of blades with corrupted data and exclusion of such blades from the final reconstruction. Hence, PROPELLER MRI is less sensitive to motion than conventional multiple-shot FSE. Furthermore, PROPELLER acquisitions are radial in nature and thus uncorrected errors are expressed in a benign fashion, similar to projection

reconstruction methods (Peters *et al.*, 2000). For these reasons, PROPELLER MRI was originally used to compensate for head motion (Forbes *et al.*, 2001) and motion of the heart in cardiac imaging with free-breathing (Pipe, 1999). Recently, DW gradients were incorporated in the PROPELLER pulse-sequence and it was shown in studies of the brain (Pipe *et al.*, 2002; Forbes *et al.*, 2002; Gui *et al.*, 2004), spinal cord (Wu *et al.*, 2003), prostate gland (Roberts *et al.*, 2004) and cartilage (Sussman *et al.*, 2004), that the results in regions with significant magnetic susceptibility differences and in objects undergoing motion were superior when using the new acquisition technique compared to conventional diffusion imaging methods. However, the imaging time in PROPELLER MRI is considerably longer than in EPI, since PROPELLER is based on multiple-shot FSE. In the most recent form of PROPELLER imaging, named Turboprop (Pipe, 2006), data acquisition is accelerated by reading out multiple lines of k-space during the spin-echo produced after each 180° pulse, similar to the gradient and spin-echo (GRASE) sequence (Oshio *et al.*, 1991). In addition to the shorter imaging time, Turboprop also allows acquisition of more lines per blade, which leads to more robust motion correction.

The purpose of this work was to compare the tractography results obtained using DTI data acquired with SE-EPI-DTI and Turboprop-DTI. Our hypothesis was that, in regions near significant magnetic field inhomogeneities, fiber-bundles mapped from data acquired with SE-EPI-DTI would be distorted and/or prematurely terminated, while the same fibers mapped from Turboprop-DTI data would be in agreement with known anatomy. In addition, we hypothesized that the inter-session reproducibility of tractography results would be lower for fibers near significant magnetic susceptibility differences when using SE-EPI-DTI than Turboprop-DTI data, due to the dependence of the artifacts in SE-EPI-DTI on head positioning. Finally, we hypothesized that the intra-session reproducibility would be higher for SE-EPI-DTI than Turboprop-DTI, due to the higher signal to noise ratio per unit time in the former compared to the latter.

Methods

MRI scans

Scans on three normal subjects were performed on a clinical 3T GE Signa MRI scanner (Waukesha, WI) with high-speed gradients (40mT/m, 150T/m/s) and the standard GE head coil. All subjects signed a consent in accordance with institutional policy. All subjects were scanned twice, on two different days. High-resolution anatomical data were acquired in both scan sessions. The 3D magnetization-prepared rapid acquisition gradient echo (MP-RAGE) sequence was used for this purpose with the following parameters: TE=3.2ms, TR=8ms, preparation time=725ms, flip angle 6°, field of view 24cm × 24cm, 124 slices, 1.5mm slice thickness, 192×256 k-space matrix reconstructed to 256×256. The scan time for this sequence was 9 minutes and 58 seconds.

In addition to the high-resolution anatomical images, two types of SE-EPI-DTI datasets were acquired in each scan session: SE-EPI-DTI$_{12}$ with 12 diffusion directions and 11 repetitions of all DW images, and SE-EPI-DTI$_{138}$ with 138 diffusion directions acquired once. Both the 12 and the 138 sets of diffusion directions belong to the “minimum energy” family of DTI acquisition schemes (Hasan *et al.*, 2001). The other scan parameters were: TR = 5400ms, TE = 71.8ms, field of view = 24cm × 24cm, 36 contiguous axial slices (same slice locations for both SE-EPI-DTI$_{12}$ and SE-EPI-DTI$_{138}$), 3mm slice thickness, 128×128 k-space matrix reconstructed to 256×256 after zero-filling, the phase encoding direction was anterior-posterior, and b=900 sec/mm^2. Images with no diffusion weighting (b=0 sec/mm^2) were also acquired at the beginning of each SE-EPI-DTI scan. For SE-EPI-DTI$_{12}$ and SE-EPI-DTI$_{138}$, 22 and 23 b=0 sec/mm^2 images were acquired respectively. High-order shimming was used in both SE-EPI-DTI$_{12}$ and SE-EPI-DTI$_{138}$ to reduce magnetic field inhomogeneities and the

corresponding EPI artifacts. The duration of the SE-EPI-DTI_{12} scan was 13 minutes and 52 seconds, and that of the SE-EPI-DTI_{138} scan was 14 minutes and 29 seconds. The calibration process that was required for high-order shimming lasted less than 2 minutes and was performed only once in each scan session.

A 2D gradient-echo sequence with two echoes, which provided the necessary output to produce maps of the phase accumulated from field inhomogeneities (Jenkinson, 2003) in SE-EPI- DTI (see data analysis section), was also included in each session. The acquisition parameters for this scan were: TE_1=5ms, TE_2=11.8ms, TR=2000ms, field of view=24cm × 24cm, 36 contiguous axial slices (same slice locations as the SE-EPI-DTI scans), 3mm slice thickness, 128×128 image matrix, and a total scan time of 4 minutes and 24 seconds. The real and imaginary components of each image were reconstructed instead of the magnitude.

Finally, a Turboprop-DTI scan was performed in each scan session. The imaging parameters for Turboprop-DTI were: TR=5000ms, TE=94ms, 8 spin-echoes per TR (ETL=8), 5 k-space lines per spin-echo (turbo-factor=5), 128 samples per line, 16 k-space blades per image, field of view=24cm × 24cm, 256×256 image matrix, 36 contiguous axial slices (same slice locations as the SE-EPI-DTI scans), and 3mm slice thickness. DW images with b=900 sec/mm^2 were acquired for the same set of 12 diffusion directions as in SE-EPI-DTI_{12}, only rotated around the z axis. Two b=0 sec/mm^2 images were also acquired. The duration of the Turboprop-DTI scan was 18 minutes and 55 seconds. This was similar to the total acquisition time for the 2D gradient-echo and SE-EPI-DTI_{12} sequences combined (18 minutes and 16 seconds), and to the total acquisition time for the 2D gradient-echo and SE-EPI-DTI_{138} sequences combined (18 minutes and 53 seconds).

In the first scan session, all subjects were asked to keep their head in the conventional position for head scanning (supine) and to maintain the same position throughout the examination. The SE-EPI-DTI_{12}, SE-EPI-DTI_{138}, and the Turboprop-DTI scans were performed twice. In the second scan session, all subjects were asked to rotate their head around the inferior-superior axis of their body, by approximately 45° to the left relative to the supine position, and maintain the same position throughout the examination. Each DTI sequence was used only once in the second scan session.

Data analysis

Pre-processing—All b=0 sec/mm^2 and b=900 sec/mm^2 image-volumes from the DTI acquisitions were first interpolated to cubic voxels with all dimensions equal to 0.9375mm, using tri-linear interpolation. Then, eddy-current-induced distortions and motion were corrected in each SE-EPI-DTI dataset separately, by registering all DW volumes to the mean DW volume, using a three-dimensional (3D), affine, 12-parameter registration algorithm (AIR 5.25, Roger Woods, UCLA, CA) (Woods *et al.*, 1998). The mean DW volume was used as a reference in the registration due to the similarity of its contrast with that of individual DW volumes, and due to the fact that the uniformly distributed diffusion directions lead to eddy-current distortions that are relatively uniformly distributed around the original object, in the phase-encoding direction.

The real and imaginary images produced for each slice with the 2D gradient-echo sequence were used to construct maps of the phase accumulated from field inhomogeneities in the SE-EPI-DTI acquisitions. The phase-maps were also interpolated to cubic voxels similar to the SE-EPI-DTI data, using tri-linear interpolation. Then, the interpolated phase-maps were used to correct susceptibility-related distortions in the SE-EPI-DTI images (Jenkinson, 2003).

Three-dimensional rigid body registration was performed on Turboprop-DTI datasets by registering each individual DW volume to the mean DW volume to correct motion between

different volumes. Following all pre-processing, five 10×10 white matter regions were selected in the b=0 sec/mm^2 images from all DTI datasets of a single subject. The mean SNR was calculated for each dataset.

Tractography—Wild bootstrap (Chung *et al.*, 2006) was performed for each of the 9 DTI datasets acquired on each subject, (two sets of SE-EPI-DTI$_{12}$, SE-EPI-DTI$_{138}$, and Turboprop-DTI data from the first scan session, and one set of SE-EPI-DTI$_{12}$, SE-EPI-DTI$_{138}$, and Turboprop-DTI data from the second scan session). Twenty wild bootstrap samples were produced for each DTI dataset of each subject. The diffusion tensors, eigenvalues and eigenvectors of the tensors, were estimated for each DTI bootstrap-sampled dataset. Trace and fractional anisotropy (FA) maps were produced (Basser, 1995). Regions of interest (ROI) were selected in all subjects, which functioned as seeds for the fiber-tracking algorithm. The streamline tracking (ST) algorithm with fiber assignment by continuous tracking (FACT) (Mori *et al.*, 1999), and the multi-ROI seeding approach (Mori *et al.*, 2002) were used in this study. The following fiber-bundles were traced for each of the 20 bootstrap samples of the 9 originally acquired DTI datasets of each subject: left fornix, corpus-callosum (CC), forceps minor (FM), left corticospinal tract (CST), left inferior and superior longitudinal fasciculi (ILF, SLF), left inferior fronto-occipital fasciculus (IFO), and left uncinate fasciculus (UF). For each fiber-bundle of interest, two ROIs were drawn at anatomical landmarks where the fibers were expected to be present (see Mori *et al.*, 2002). Only fibers that passed through both ROIs were retained. The ROIs were drawn on high-resolution T_1-weighted data that were first coregistered to each original DTI dataset from the first scan session (6 DTI datasets were included in the first scan session, therefore 6 coregistered T_1-weighted datasets were produced, and 6 sets of ROIs were drawn for each tract of each subject). To eliminate the dependence of the tracking results on the ROI selection, the size of all ROIs was rather large, and in several cases as large as the cross-section of a whole brain lobe with a certain plane (see Mori *et al.*, 2002). Furthermore, the ROIs used on the DTI data from the second scan session were obtained by spatial transformation of the ROIs selected on the data from the first session, according to transformation parameters obtained by registering DTI data of the same type (i.e. SE-EPI-DTI or Turboprop-DTI) between sessions. In the SLF, only one seed region was selected similar to previously published work (Mori *et al.*, 2002). Tracts were terminated when a voxel with FA lower than 0.2 was reached, or when the change in orientation of the primary eigenvector between two steps of the tracking algorithm was larger than 45°.

All fiber-bundles produced using the tractography algorithm originally consisted of thin lines with width equal to that of a single voxel from the interpolated DTI data. For the rest of the analysis, 3D volumetric representations of the bundles were used instead. These were created as follows. First, planes almost perpendicular to a fiber-bundle were selected (Lazar *et al.*, 2005). The cross-section of the fiber-lines with each plane defined “fiber-points” (Fig. 1A). Same-plane “fiber-points” separated by less than 3 voxels from each other were assigned to the same cluster (Fig. 1B). The vertices of the minimum perimeter polygon that contained all the “fiber-points” in each cluster were identified (Fig. 1C). Then, 100 points were selected uniformly along each side of the minimum perimeter polygon, and the “fiber-points” closer to each one of the 100 points were identified. Subsequently, these “fiber-points” were connected to each other in the same plane, and the original side of the polygon was substituted with a more complex line (Fig. 1D). The same process was repeated for the whole length of the fiber-bundle, therefore creating a volumetric representation of the tract. All the voxels enclosed in this structure were considered part of that fiber-bundle for the rest of the analysis (Fig. 1E).

Reproducibility of tractography results—The intra-session reproducibility of tractography results was assessed for SE-EPI-DTI$_{12}$, SE-EPI-DTI$_{138}$, and Turboprop-DTI. In the first scan session, two original datasets were acquired with each sequence, and for each original dataset 20 bootstrap-sampled datasets and 20 copies of each fiber-bundle were

produced. Intra-session reproducibility was assessed by comparing the 20 copies of a tract produced from one original DTI dataset to the 20 copies of the same tract produced from the second dataset of the same type. For that purpose, the b=0 sec/mm^2 image volume from the first SE-EPI-DTI$_{12}$ dataset of the first scan session, was registered to the b=0 sec/mm^2 image volume from the second SE-EPI-DTI$_{12}$ dataset of the first session, using 3D rigid body registration (AFNI, Robert Cox, NIH, Bethesda, MD). The same procedure was followed for the SE-EPI-DTI$_{138}$ and Turboprop-DTI data. The registration parameters were then applied to the tracts produced from one copy of each dataset in order to match the tracts produced from the second dataset of the same type. The ratio of the number of common voxels between two homologous fiber-pathways produced from two datasets of the same type, over the total number of voxels that belong to at least one of the two fiber-pathways, was estimated for all three types of DTI acquisitions and all fiber-tracts under study. Finally, the inter-session reproducibility of tractography results was assessed following similar procedures as for the intra-session reproducibility, with the only difference that comparisons were made using bootstrap-sampled data produced from two original datasets acquired with the same method in two different scan sessions. Twenty estimates of intra-session and inter-session reproducibility were obtained for all three data acquisition schemes (SE-EPI-DTI$_{12}$, SE-EPI-DTI$_{138}$, Turboprop-DTI). A paired t-test was employed to assess statistically significant differences in reproducibility between the three acquisition schemes, for all fiber-tracts. Statistical significance was determined at $p<0.05$.

Results

Pre-processing

Eddy-current-induced distortions in the SE-EPI-DTI data were significantly reduced following 3D registration of all DW volumes to the mean DW volume. However, these images and the corresponding DTI maps contained significant magnetic-susceptibility-related distortions, signal loss and signal hyperintensities, in the frontal and temporal lobes and the brainstem (Fig. 2). After correction using the phase maps, the susceptibility artifacts were reduced but remained significant (Fig. 2). In contrast, raw images acquired with Turboprop-DTI, and the corresponding DTI maps, were free of eddy-current and susceptibility-related artifacts. The mean SNR in white matter, as estimated from the b=0 sec/mm^2 images of a single subject following all pre-processing, was 57±12 for SE-EPI-DTI$_{12}$, 50±7 for SE-EPI-DTI$_{138}$, and 24 ±10 for Turboprop-DTI.

Tractography

Fiber-tracking using the SE-EPI-DTI data prior to magnetic susceptibility-related distortion correction was problematic. For example, when tracking the anterior commissure (AC) in a normal subject using uncorrected SE-EPI-DTI$_{12}$ data and seed regions near the middle sagittal slice, only a small portion of the fiber-bundle was mapped (Fig. 3A). After rearranging the seeds and restarting the fiber-tracking algorithm, the result remained relatively unchanged. In contrast, the pathway obtained from the Turboprop-DTI data was a more complete representation of the AC (Fig. 3B). Careful inspection of the FA maps from the two datasets revealed that the most superior part of the AC was significantly distorted in the SE-EPI-DTI$_{12}$ dataset. More specifically, the part of the AC that is contained in the axial slice shown in Figure 3C was characterized by significantly increased curvature (Fig. 3C, D). However, although the shape of the fiber-bundle was modified, the diffusion information in the voxels inside the AC remained approximately the same. Thus, after distortion, the orientation of the primary eigenvectors within the AC did not correspond to the increased curvature of the fiber-bundle. As a result, the estimated pathway was not curved enough during the fiber-tracking procedure, reached the walls of the bundle, and was terminated prematurely. A more complete tract was obtained after distortion correction. Similar effects may occur in any tract that is near

significant field inhomogeneities. Therefore, in this study, SE-EPI-DTI data were used only after correction of magnetic susceptibility-related distortions.

Fibers produced from SE-EPI-DTI_{12}, SE-EPI-DTI_{138} and Turboprop-DTI data are displayed in Figure 4, using FA maps from each acquisition method as background. Overlays of fibers produced from SE-EPI-DTI and Turboprop-DTI datasets showed that in brain regions distant from B_0 inhomogeneities, fibers from the two DTI data types appeared similar. In contrast, tracts located near magnetic-susceptibility differences appeared distorted and in some subjects incomplete when using SE-EPI-DTI data (depending on the amount of residual image distortions and artifacts). These effects were visible in fibers such as the FM, ILF, IFO, UF, and the inferior part of the CST. Similar results were obtained for tracts in both hemispheres and in all subjects. Subject motion between sequences was minimal and was corrected before performing any comparisons, as described in the methods section.

Reproducibility of tractography results

The intra-session reproducibility of tracking results was generally higher for SE-EPI-DTI_{138} than Turboprop-DTI, and comparable for SE-EPI-DTI_{12} and Turboprop-DTI, in all subjects (Table 1, Table 2, Table 3) (Fig. 5). The inter-session reproducibility of tracking results was in general higher for Turboprop-DTI than SE-EPI-DTI_{12} and SE-EPI-DTI_{138} in fiber-bundles near field inhomogeneities, such as the ILF, FM, UF and part of the CST, in all subjects (Table 4, Table 5, Table 6) (Fig. 5, Fig. 6). In the fornix, the inter-session reproducibility was significantly lower in Turboprop-DTI compared to SE-EPI-DTI_{12} in subject 1 (Table 4), and significantly lower compared to SE-EPI-DTI_{138} for subject 2 (Table 5). However, in these subjects, the crus of the fornix reconstructed from SE-EPI-DTI data was characterized by distorted and early-terminated fibers (Fig. 6). No consistent difference was identified in the inter-session reproducibility of the IFO between Turboprop-DTI, SE-EPI-DTI_{12}, and SE-EPI-DTI_{138}, for the group of subjects studied (Table 5). The intra and inter-session reproducibility of tracking results were not estimated for the CC and SLF due to significant fanning which may introduce errors.

Discussion

The development of accurate, non-invasive methods to map white matter fiber-tracts is of critical importance. Knowledge of the exact location of eloquent white matter pathways with respect to a lesion is of great value to neurosurgeons in planning the appropriate surgical strategy. Accurate and reproducible mapping of white matter fiber-tracts is also crucial when comparing patients with neurological abnormalities to healthy controls, when monitoring the progression of disease longitudinally, or when studying normal neuronal networks. For these reasons, several tractography algorithms have been developed to optimize the tracking procedure. However, the accuracy and reproducibility of tractography results also depend on the noise level and amount of artifacts of the DTI data. Therefore, this study focused on comparing tracking results obtained from distortion-corrected SE-EPI-DTI and Turboprop-DTI datasets.

Image registration successfully removed most of the distortions due to eddy currents in the SE-EPI-DTI images. However, two additional scans (high order shimming, 2D gradient-echo with two echoes) and further image-processing were necessary to reduce magnetic susceptibility-related effects. Although the improvement was significant, residual artifacts were visible when comparing the corrected SE-EPI-DTI images to high-resolution anatomical data. Several methods have been proposed that can reduce susceptibility-related artifacts in SE-EPI-DTI (Young *et al.*, 1988; Wan *et al.*, 1997; Chen *et al.*, 2001; Kadah *et al.*, 1997; Chiou *et al.*, 2003; Schneider *et al.*, 1991; Jezzard *et al.*, 1995; Reber *et al.*, 1998; Zeng *et al.*, 2002; Robson *et al.*, 1997; Andersson *et al.*, 2003; Jiang *et al.*, 2002; Bammer *et al.*, 2002; Blaimer *et al.*,

2004; Ohliger *et al.*, 2003). The method used here provides significantly improved images, is simple to implement, and was preferred over techniques that increase the total scan time, or are computationally intensive, or both. However, although some methods perform better than others, most of the available techniques do not completely correct susceptibility-induced artifacts. Segmented EPI can reduce susceptibility artifacts to a great extent, but was not used here since it is sensitive to motion, even when using navigator echoes (Jiang *et al.*, 2002). Also, in order to reduce susceptibility artifacts to the same degree as the Turboprop sequence used here, k-space would have to be divided in multiple segments (approximately 20), which would significantly increase the total acquisition time (to a time higher than that of Turboprop). Parallel imaging can also reduce susceptibility artifacts to a great extent (Bammer *et al.*, 2002; Blaimer *et al.*, 2004; Ohliger *et al.*, 2003). Parallel imaging was not available on the MRI system at the time the current study was performed. However, in order to reduce susceptibility artifacts to the same degree as Turboprop-DTI, high acceleration factors (on the order of 20) would have to be used. The limiting factor in this case is that for clinical 2D brain imaging applications the acceleration factor is not expected to exceed a factor of 4 or 5 (due to significant noise amplification for higher acceleration factors) (Blaimer *et al.*, 2004; Ohliger *et al.*, 2003). Also, the vast majority of investigations that perform SE-EPI-DTI scans with parallel imaging use an acceleration factor of 2, which slightly limits signal loss, but in general provides data that are not significantly different than the corrected SE-EPI-DTI data used in this study. Therefore, the fact that a combination of high-order shimming and distortion correction using field-maps was used in the present investigation, instead of parallel imaging, should not significantly affect the fact that, Turboprop-DTI with low turbofactors (and no additional scans or corrections) provides DTI data that are superior in terms of distortions and artifacts than SE-EPI-DTI combined with any of the corrections listed above. This characteristic of Turboprop-DTI is crucial for tractography, since residual distortions and artifacts in DTI data may introduce errors in tracking results.

The intra-session reproducibility of tracking results was higher when using SE-EPI-DTI_{138} than Turboprop-DTI data (Table 1, Table 2, Table 3) (Fig. 5). This was due to the significantly higher SNR in SE-EPI-DTI_{138} compared to Turboprop-DTI datasets (more than two times higher SNR for approximately the same total scan time). The shorter TE and the higher amount of data acquired per unit time in SE-EPI-DTI_{138} compared to Turboprop-DTI, were the primary reasons for the severe discrepancy in SNR. In fibers located away from field inhomogeneities, the higher intra-session reproducibility in SE-EPI-DTI_{138} compared to Turboprop-DTI means that, fiber-tracking based on the former provides more reproducible results than the latter. However, for fibers near field inhomogeneities, higher intra-session reproducibility means that a tract that is distorted, partially traced, or prematurely terminated will be mapped in a reproducible manner as long as the positioning of the head remains the same. Finally, the intra-session reproducibility did not approach 100% for any of the acquisition techniques used in this study due to the presence of noise in all DTI datasets.

The inter-session reproducibility was in general higher in Turboprop-DTI compared to SE-EPI-DTI_{12} and SE-EPI-DTI_{138}, in fiber-bundles near field inhomogeneities (Table 4, Table 5, Table 6) (Fig. 5, Fig. 6). This was due to the fact that susceptibility-related artifacts are expressed in a unique manner in SE-EPI-DTI images for each positioning of the brain in the scanner. Altering the positioning between scans, alters the influence of susceptibility variations on the shape and location of fibers. This is demonstrated in the left two columns of Figure 6, where CST, ILF, and FM fibers produced from SE-EPI-DTI datasets, acquired in different sessions with different head positioning, are significantly mismatched. In contrast, in the IFO, no consistent difference was identified in the inter-session reproducibility of tracking results between Turboprop-DTI, SE-EPI-DTI_{12}, and SE-EPI-DTI_{138}, for the group of subjects studied. This was due to the fact that the IFO is relatively removed from susceptibility variations, and any field inhomogeneity effects on the IFO were corrected. Therefore,

Turboprop-DTI data acquisitions may be more appropriate for longitudinal studies of white matter fiber-bundles that are near magnetic field inhomogeneities.

The inter-session reproducibility of tracking results for SE-EPI-DTI$_{12}$ and SE-EPI-DTI$_{138}$ was significantly reduced compared to the intra-session reproducibility, for fibers near susceptibility-related artifacts (Table 1–Table 6) (Fig. 5). For some fiber-bundles, this reduction was as high as 50%, demonstrating the magnitude of the errors that could be introduced in longitudinal studies that use SE-EPI-DTI acquisitions for fiber-tracking near susceptibility artifacts. In contrast, the inter-session reproducibility of fiber-tracking results for Turboprop-DTI was slightly lower than, but very similar to, the intra-session reproducibility (Table 1–Table 6) (Fig. 5). However, the inter and intra-session reproducibilities of tracking results in Turboprop-DTI are lower than the intra-session reproducibility of fibers in SE-EPI-DTI due to the higher noise content of the Turboprop-DTI data. Therefore, SE-EPI-DTI may be more appropriate than Turboprop-DTI for longitudinal or cross-sectional studies performing tractography in regions distant from susceptibility artifacts, due to the significantly higher SNR of the former compared to the latter. Further research is necessary in order to reduce the noise levels of Turboprop-DTI data.

Intra-session and inter-session reproducibility of tracking results based on SE-EPI-DTI$_{138}$ were generally higher than for SE-EPI-DTI$_{12}$ (Table 1–Table 6). This was partly due to the almost 12 times more diffusion directions used in SE-EPI-DTI$_{138}$ compared to SE-EPI-DTI$_{12}$. Furthermore, the 11 repetitions of each DW image in SE-EPI-DTI$_{12}$ may have contained motion that remained uncorrected after averaging. In contrast, in SE-EPI-DTI$_{138}$ acquisitions, one copy of each diffusion-weighted volume was obtained, and the 3D registration used to correct the effects of eddy-currents also corrected any motion between diffusion directions.

Wild bootstrap (Chung *et al.*, 2006) was used in this study. When applied to DTI experiments with a low number of diffusion directions, wild bootstrap can introduce a high overall sampling bias in the estimation of the primary eigenvector of the diffusion tensor. This may have slightly increased the reproducibility of tractography results using SE-EPI-DTI$_{138}$ compared to SE-EPI-DTI$_{12}$ or Turboprop-DTI data.

The volumetric representation of fiber-bundles, which was used in the comparisons between homologous tracts, provided only an approximation of a bundle's shape and size. Furthermore, the volumetric representations of bundles may have contained fibers that belonged to different tracts. However, none of these imperfections could have significantly affected the results of the investigation on the effects of distortions and artifacts on tracking results. Thus, comparing the volumetric representations of tracts allows detection of distorted or prematurely terminated fiber-bundles.

Cardiac gating was not used in any of the DTI data acquisitions performed in this study. Brain pulsation occurring during the diffusion encoding period causes an increase in signal attenuation, an overestimation of the diffusivity along different diffusion gradient directions, and leads to erroneous diffusion tensors and principal eigenvectors. These effects are independent of the excitation, refocusing, and signal readout periods of a DTI sequence and have been observed in diffusion imaging studies using EPI (Pierpaoli *et al.*, 2003; Brockstedt *et al.*, 1999; Skare *et al.*, 2001), segmented EPI (Jiang *et al.*, 2002; Brockstedt *et al.*, 2000), spin-echo (Wirestam *et al.*, 1996), stimulated echo acquisition mode (STEAM) (Merboldt *et al.*, 1992), fast low angle shot (FLASH), projection reconstruction, line scanning, FSE (Dietrich *et al.*, 2000), and recently, Turboprop sequences (Gui *et al.*, 2008). Thus, we do not expect the lack of cardiac gating to bias the results of this study.

The comparisons presented here were performed based on data acquired from healthy human subjects. According to our experience, the corrected SE-EPI-DTI datasets in this study

contained susceptibility-related effects of minor severity. In patients with intracranial hemorrhage, post-surgical metal plates, valves to control pressure in the case of hydrocephalus, etc., magnetic susceptibility-related artifacts in SE-EPI-DTI can be significantly enhanced. It is therefore apparent that, the differences in intra-session and inter-session reproducibility of tracking results between SE-EPI-DTI and Turboprop-DTI presented in this study are not representative of all cases. The purpose of the comparisons presented here was to demonstrate that the decision on the acquisition method to be used for a tractography study should be guided by an evaluation of the level of field inhomogeneities in the brain region of interest.

In conclusion, in brain regions near significant field inhomogeneities, fiber-tracts produced using Turboprop-DTI datasets were in better agreement with the anatomy than tracts produced from corrected SE-EPI-DTI data. No additional scans or corrections of distortions and artifacts were necessary for Turboprop-DTI data. The intra-session reproducibility of tracking results was higher for SE-EPI-DTI$_{138}$ due to the lower noise content compared to Turboprop-DTI acquisitions. The inter-session reproducibility of tracking results near magnetic susceptibility differences was higher for Turboprop-DTI due to the susceptibility-related distortions and artifacts in SE-EPI-DTI data, which depend on the positioning of the subject's head. Further research is necessary in order to reduce the noise content of Turboprop-DTI data.

Acknowledgements

This work was supported by a grant from the National Institute of Biomedical Imaging and Bioengineering (NIBIB) 1R21EB005273-01, and an Interdisciplinary Seed Funding Grant from the Pritzker Institute of Biomedical Science and Engineering.

References

Alexander AL, Tsuruda JS, Parker DL. Elimination of eddy current artifacts in diffusion-weighted echo planar images: the use of bipolar gradients. Magn Reson Med 1997;38:1016–1021. [PubMed: 9402204]

Andersson JL, Skare S, Ashburner J. How to correct susceptibility distortions in spin-echo echo-planar images: application to diffusion tensor imaging. Neuroimage 2003;20:870–888. [PubMed: 14568458]

Bammer R, Auer M, Keeling SL, Augustin M, Stables LA, Prokesch RW, Stollberger R, Moseley ME, Fazekas F. Diffusion tensor imaging using single-shot SENSE-EPI. Magn Reson Med 2002;48:128–136. [PubMed: 12111940]

Basser PJ, Mattiello J, Le Bihan D. Estimation of the effective self-diffusion tensor from the NMR spin echo. J Magn Reson B 1994;103:247–254. [PubMed: 8019776]

Basser PJ. Inferring microstructural features and the physiological state of tissues from diffusion-weighted images. NMR in Biomedicine 1995;8:333–344. [PubMed: 8739270]

Basser PJ, Pajevic S, Pierpaoli C, Duda J, Aldroubi A. In vivo tractography using DT-MRI data. Magn Reson Med 2000;44:625–632. [PubMed: 11025519]

Behrens TE, Woolrich MW, Jenkinson M, Johansen-Berg H, Nunes RG, Clare S, Matthews PM, Brady JM, Smith SM. Characterization and propagation of uncertainty in diffusion-weighted MR imaging. Magn Reson Med 2003;50:1077–1088. [PubMed: 14587019]

Berman JI, Berger MS, Mukherjee P, Henry RG. Diffusion-tensor imaging-guided tracking of fibers of the pyramidal tract combined with intraoperative cortical stimulation mapping in patients with gliomas. J Neurosurg 2004;101:66–72. [PubMed: 15255253]

Blaimer M, Breuer F, Mueller M, Heidemann RM, Griswold MA, Jakob PM. SMASH, SENSE, PILS, GRAPPA: how to choose the optimal method. Top Magn Reson Imaging 2004;15:223–236. [PubMed: 15548953]

Brockstedt S, Borg M, Geijer B, Wirestam R, Thomsen C, Holtas S, Stahlberg F. Triggering in quantitative diffusion imaging with single-shot EPI. Acta Radiologica 1999;40:63–269.

Brockstedt S, Moore JR, Thomsen C, Holtas S, Stahlberg F. High-resolution diffusion imaging using phase-corrected segmented echo-planar imaging. Magn Reson Imaging 2000;18:649–657. [PubMed: 10930774]

Butts K, de Crespigny A, Pauly JM, Moseley M. Diffusion-weighted interleaved echo-planar imaging with a pair of orthogonal navigator echoes. Magn Reson Med 1996;35:763–770. [PubMed: 8722828]

Catani M, Howard RJ, Pajevic S, Jones DK. Virtual in vivo interactive dissection of white matter fasciculi in the human brain. Neuroimage 2002;17:77–94. [PubMed: 12482069]

Chen NK, Wyrwicz AM. Optimized distortion correction technique for echo planar imaging. Magn Reson Med 2001;45:525–528. [PubMed: 11241714]

Chiou JY, Ahn CB, Muftuler LT, Nalcioglu O. A simple simultaneous geometric and intensity correction method for echo-planar imaging by EPI-based phase modulation. IEEE Trans Med Imaging 2003;22:200–205. [PubMed: 12715996]

Chung SW, Lu Y, Henry RG. Comparison of bootstrap approaches for estimation of uncertainties of DTI parameters. Neuroimage 2006;33:531–541. [PubMed: 16938472]

Clark CA, Barrick TR, Murphy MM, Bell BA. White matter fiber tracking in patients with space-occupying lesions of the brain: a new technique for neurosurgical planning. Neuroimage 2003;20:1601–1608. [PubMed: 14642471]

Concha, L.; Gross, DW.; Beaulieu, C. Proceedings of the ISMRM Twelfth Scientific Meeting. Kyoto, Japan: 2004. Diffusion tensor imaging tractography using fluid-attenuated inversion recovery; p. 1194

Conturo TE, Lori NF, Cull TS, Akbudak E, Snyder AZ, Shimony JS, McKinstry RC, Burton H, Raichle ME. Tracking neuronal fiber pathways in the living human brain. Proc Natl Acad Sci 1999;96:10422–10427. [PubMed: 10468624]

Dietrich O, Heiland S, Benner T, Sartor K. Reducing motion artifacts in diffusion-weighted MRI of the brain: efficacy of navigator echo correction and pulse triggering. Neuroradiology 2000;42:85–91. [PubMed: 10663480]

Forbes KP, Pipe JG, Bird CR, Heiserman JE. PROPELLER MRI: Clinical testing of a novel technique for quantification and compensation of head motion. J Magn Reson Imaging 2001;14:215–222. [PubMed: 11536397]

Forbes KP, Pipe JG, Karis JP, Heiserman JE. Improved image quality and detection of acute cerebral infarction with PROPELLER diffusion-weighted MR imaging. Radiology 2002;225:551–555. [PubMed: 12409594]

Gui, M.; Lazar, M.; Arfanakis, K. Proceedings of the ISMRM Twelfth Scientific Meeting. Kyoto, Japan: 2004. A Comparison of White Matter Fiber-Tracking Results Using PROPELLER and SE-EPI Datasets; p. 1283

Gui M, Tamhane AA, Arfanakis K. Contribution of Cardiac-Induced Brain Pulsation to the Noise of the Diffusion Tensor in Turboprop diffusion tensor imaging (DTI). J Magn Reson Imaging 2008;27:1164–1168. [PubMed: 18425837]

Guye M, Parker GJ, Symms M, Boulby P, Wheeler-Kingshott CA, Salek-Haddadi A, Barker GJ, Duncan JS. Combined functional MRI and tractography to demonstrate the connectivity of the human primary motor cortex in vivo. Neuroimage 2003;19:1349–1360. [PubMed: 12948693]

Hasan KM, Parker DL, Alexander AL. Comparison of gradient encoding schemes for diffusion-tensor MRI. J Magn Reson Imaging 2001;13:769–780. [PubMed: 11329200]

Henry RG, Berman JI, Nagarajan SS, Mukherjee P, Berger MS. Subcortical pathways serving cortical language sites: initial experience with diffusion tensor imaging fiber tracking combined with intraoperative language mapping. Neuroimage 2004;21:616–622. [PubMed: 14980564]

Huang H, Zhang J, van Zijl PCM, Mori S. Analysis of noise effects on DTI-based tractography using the brute-force and multi-ROI approach. Magn Reson Med 2004;52:559–565. [PubMed: 15334575]

Jenkinson M. Fast, automated, N-dimensional phase-unwrapping algorithm. Magn Reson Med 2003;49:193–197. [PubMed: 12509838]

Jezzard P, Balaban RS. Correction for geometric distortion in echo planar images from B0 field variations. Magn Reson Med 1995;34:65–73. [PubMed: 7674900]

Jiang H, Golay X, van Zijl PCM, Mori S. Origin and minimization of residual motion-related artifacts in navigator-corrected segmented diffusion-weighted EPI of the human brain. Magn Reson Med 2002;47:818–822. [PubMed: 11948746]

Jones DK, Pierpaoli C. Confidence mapping in diffusion tensor magnetic resonance imaging tractography using a bootstrap approach. Magn Reson Med 2005;53:1143–1149. [PubMed: 15844149]

Jones DK, Simmons A, Williams SCR, Horsfiled MA. Noninvasive assessment of axonal fiber connectivity in the human brain via diffusion tensor MRI. Magn Reson Med 1999;42:37–41. [PubMed: 10398948]

Kadah YM, Hu X. Simulated phase evolution rewinding (SPHERE): a technique for reducing B0 inhomogeneity effects in MR images. Magn Reson Med 1997;38:615–627. [PubMed: 9324329]

Koch MA, Norris DG, Hund-Georgiadis M. An investigation of functional and anatomical connectivity using magnetic resonance imaging. Neuroimage 2002;16:241–250. [PubMed: 11969331]

Lazar M, Weinstein DM, Tsuruda JS, Hasan KM, Arfanakis K, Meyerand ME, Badie B, Rowley HA, Haughton V, Field A, Alexander AL. White matter tractography using diffusion tensor deflection. Hum Brain Mapp 2003;18:306–321. [PubMed: 12632468]

Lazar M, Alexander AL. Bootstrap white matter tractography (BOOT-TRAC). Neuroimage 2005;24:524–532. [PubMed: 15627594]

Le Bihan D, Mangin JF, Poupon C, Clark CA, Pappata S, Molko N, Chabriat H. Diffusion tensor imaging: concepts and applications. J Magn Reson Imaging 2001;13:534–546. [PubMed: 11276097]

Lori NF, Akbudak E, Shimony JS, Cull TS, Snyder AZ, Guillory RK, Conturo TE. Diffusion tensor fiber tracking of human brain connectivity: aquisition methods, reliability analysis and biological results. NMR Biomed 2002;15:494–515. [PubMed: 12489098]

Merboldt KKD, Hanicke W, Bruhn H, Gyngell ML, Frahm J. Diffusion imaging of the human brain in vivo using high-speed STEAM MRI. Magn Reson Med 1992;23:179–192. [PubMed: 1734178]

Mori S, Crain B, Chacko VP, van Zijl PCM. Three-dimensional tracking of axonal projections in the brain by magnetic resonance imaging. Ann Neurol 1999;45:265–269. [PubMed: 9989633]

Mori S, Kaufmann WE, Davatzikos C, Stieljes B, Amodei L, Fredericksen K, Pearlson GD, Melhem ER, Solaiyappan M, Raymond GV, Moser HW, van Zijl PC. Imaging cortical association tracts in the human brain using diffusion-tensor-based axonal tracking. Magn Reson Med 2002;47:215–223. [PubMed: 11810663]

Ohliger MA, Grant AK, Sodickson DK. Ultimate intrinsic signal-to-noise ratio for parallel MRI: electromagnetic field considerations. Magn Reson Med 2003;50:1018–1030. [PubMed: 14587013]

Oshio K, Feinberg DA. GRASE (Gradient- and spin-echo) imaging: a novel fast MRI technique. Magn Reson Med 1991;20:344–349. [PubMed: 1775061]

Parker GJM, Haroon HA, Wheeler-Kingshott CAM. A framework for a streamline-based probabilistic index of connectivity (PICo) using a structural interpretation of MRI diffusion measurements. J Magn Reson Imaging 2003;18:242–254. [PubMed: 12884338]

Peters DC, Korosec FR, Grist TM, Block WF, Holden JE, Vigen KK, Mistretta CA. Undersampled projection reconstruction applied to MR angiography. Magn Reson Med 2000;43:91–101. [PubMed: 10642735]

Pierpaoli C, Basser PJ. Toward a quantitative assessment of diffusion anisotropy. Magn Reson Med 1996;36:893–906. [PubMed: 8946355]

Pierpaoli, C.; Marenco, S.; Rohde, G.; Jones, DK.; Barnett, AS. Proceedings of the ISMRM Eleventh Scientific Meeting. Toronto, Canada: 2003. Analyzing the contribution of cardiac pulsation to the variability of quantities derived from the diffusion tensor; p. 70

Pipe JG. Motion correction with PROPELLER MRI: Application to head motion and free-breathing cardiac imaging. Magn Reson Med 1999;42:963–969. [PubMed: 10542356]

Pipe JG, Farthing VG, Forbes KP. Multishot diffusion-weighted FSE using PROPELLER MRI. Magn Reson Med 2002;47:42–52. [PubMed: 11754441]

Pipe JG, Zwart N. Turboprop: improved PROPELLER imaging. Magn Reson Med 2006;55:380–385. [PubMed: 16402378]

Poupon C, Clark CA, Frouin V, Regis J, Bloch I, Le Bihan D, Mangin J. Regularization of diffusion-based direction maps for the tracking of brain white matter fascicles. Neuroimage 2000;12:184–195. [PubMed: 10913324]

Reber PJ, Wong EC, Buxton RB, Frank LR. Correction of off resonance-related distortion in echo-planar imaging using EPI-based field maps. Magn Reson Med 1998;39:328–330. [PubMed: 9469719]

Roberts, TP.; Haider, M. Proceedings of the ISMRM Twelfth Scientific Meeting. Kyoto, Japan: 2004. Diffusion weighted imaging of the prostate gland in the face of magnetic susceptibility differences – Parallel EPI and PROPELLER FSE approaches.

Robson MD, Gore JC, Constable RT. Measurement of the point spread function in MRI using constant time imaging. Magn Reson Med 1997;38:733–740. [PubMed: 9358447]

Schneider E, Glover G. Rapid in vivo proton shimming. Magn Reson Med 1991;18:335–347. [PubMed: 2046515]

Skare S, Anderson JLR. On the effects of gating in diffusion imaging of the brain using single shot EPI. Magn Reson Imaging 2001;19:1125–1128. [PubMed: 11711237]

Stieltjes B, Kaufmann WE, van Zijl PCM, Fredericksen K, Pearlson GD, Solaiyappan M, Mori S. Diffusion tensor imaging and axonal tracking in the human brain. Neuroimage 2001;14:723–735. [PubMed: 11506544]

Sussman, MS.; White, LM.; Roberts, TP. Proceedings of the ISMRM Twelfth Scientific Meeting. Kyoto, Japan: 2004. High-resolution diffusion-weighted imaging of cartilage using PROPELLER; p. 211

Tench CR, Morgan PS, Wilson M, Blumhardt LD. White matter mapping using diffusion tensor MRI. Magn Reson Med 2002;47:967–972. [PubMed: 11979576]

Toosy AT, Ciccarelli O, Parker GJ, Wheeler-Kingshott CA, Miller DH, Thompson AJ. Characterizing function-structure relationships in the human visual system with functional MRI and diffusion tensor imaging. Neuroimage 2004;21:1452–1463. [PubMed: 15050570]

Wan X, Gullberg GT, Parker DL, Zeng GL. Reduction of geometric and intensity distortions in echo-planar imaging using a multireference scan. Magn Reson Med 1997;37:932–942. [PubMed: 9178246]

Wirestam R, Greitz D, Thomsen C, Brockstedt S, Olsson MBE, Stahlberg F. Theoretical and experimental evaluation of phase-dispersion effects caused by brain motion in diffusion and perfusion MR imaging. J Magn Reson Imaging 1996;6:348–355. [PubMed: 9132101]

Woods RP, Grafton ST, Holmes CJ, Cherry SR, Mazziotta JC. Automated image registration: I. General methods and intrasubject, intramodality validation. J Comp Assist Tomogr 1998;22:141–154.

Wu, Y.; Field, AS.; Alexander, AL. Proceedings of the ISMRM Eleventh Scientific Meeting. Toronto, Canada: 2003. Diffusion tensor imaging of the human cervical spinal cord using PROPELLER; p. 2125

Young IR, Cox IJ, Bryant DJ, Bydder GM. The benefits of increasing spatial resolution as a means of reducing artifacts due to field inhomogeneities. Magn Reson Imaging 1988;6:585–590. [PubMed: 3226241]

Zeng H, Constable RT. Image distortion correction in EPI: comparison of field mapping with point spread function mapping. Magn Reson Med 2002;48:137–146. [PubMed: 12111941]

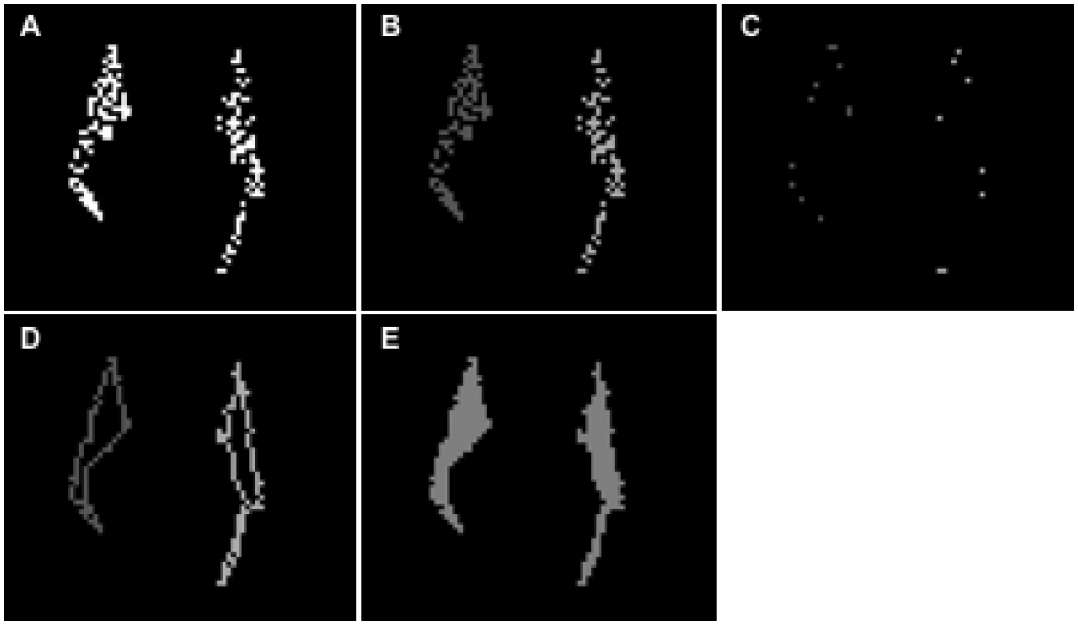

Figure 1.

A) Cross-section of the fibers of the forceps-minor with a coronal plane. The white dots represent voxels that belong to fiber-lines. These voxels are referred to in the text as “fiber-points”. B) The “fiber-points” of the forceps-minor that belong to the left and right hemispheres are assigned to different clusters. The cluster corresponding to the right hemisphere is shaded darker grey and the one corresponding to the left hemisphere is shaded lighter grey. C) The vertices of the minimum perimeter polygons that enclose all the “fiber-points” in each cluster. D) The complex lines that connect the “fiber-points” closer to the sides of the minimum perimeter polygons. E) The voxels that were eventually considered to be part of the volumetric representation of this fiber-bundle.

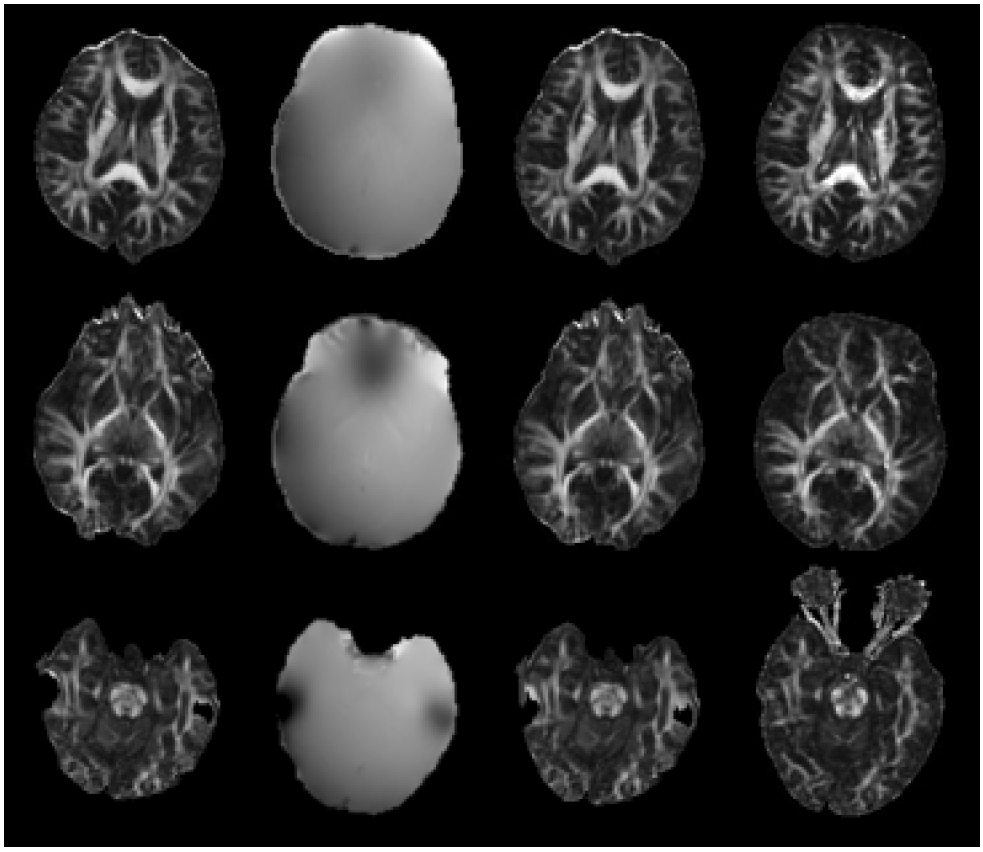

Figure 2.
Each row in this figure corresponds to a different slice of a normal volunteer. The first column contains FA maps produced from SE-EPI-DTI_{12} data (after correction of eddy-current distortions). The second column contains the corresponding unwrapped phase-maps. The third column contains FA maps produced from SE-EPI-DTI_{12} data that have been corrected for susceptibility-related distortions. The last column contains FA maps produced from Turboprop-DTI data. Distortions, signal loss and signal hyperintensities are visible in the SE-EPI-DTI_{12} images near tissue-bone and tissue-air interfaces, even after correction using the phase maps. In regions distant to significant magnetic field inhomogeneities, the distortions in SE-EPI-DTI_{12} images are not as pronounced. Turboprop-DTI images are free of eddy-current and susceptibility related artifacts.

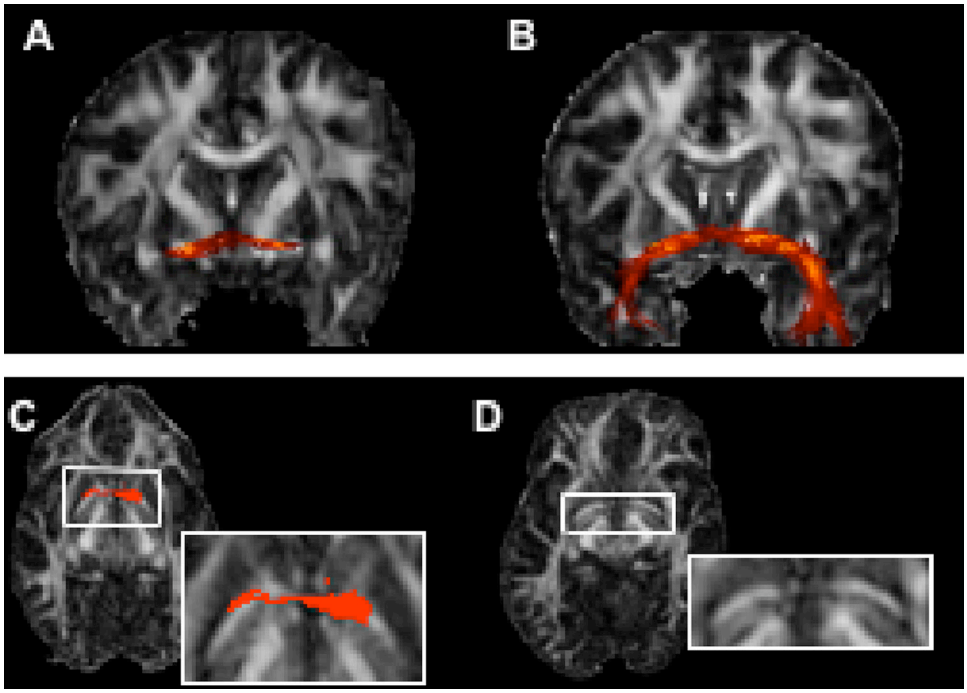

Figure 3.

Fibers of the AC, reconstructed from SE-EPI-DTI$_{12}$ (before distortion correction) (A) and Turboprop-DTI (B) data from the same subject. Tracking based on SE-EPI-DTI$_{12}$ data mapped only part of the AC (A). Tracking based on Turboprop-DTI data produced a more complete representation of the AC (B). The part of the AC that is included in the axial slice shown in C and D is characterized by increased curvature in SE-EPI-DTI$_{12}$ (C), compared to Turboprop-DTI (D), due to magnetic susceptibility-related distortions. The cross-section of the traced AC fibers with this axial plane is shown in red. Although the curvature of the AC is increased due to the distortions, the diffusion orientation information within the AC remains the same. Thus, the estimated pathway was not curved enough during the fiber-tracking procedure, reached the walls of the bundle, and was terminated prematurely.

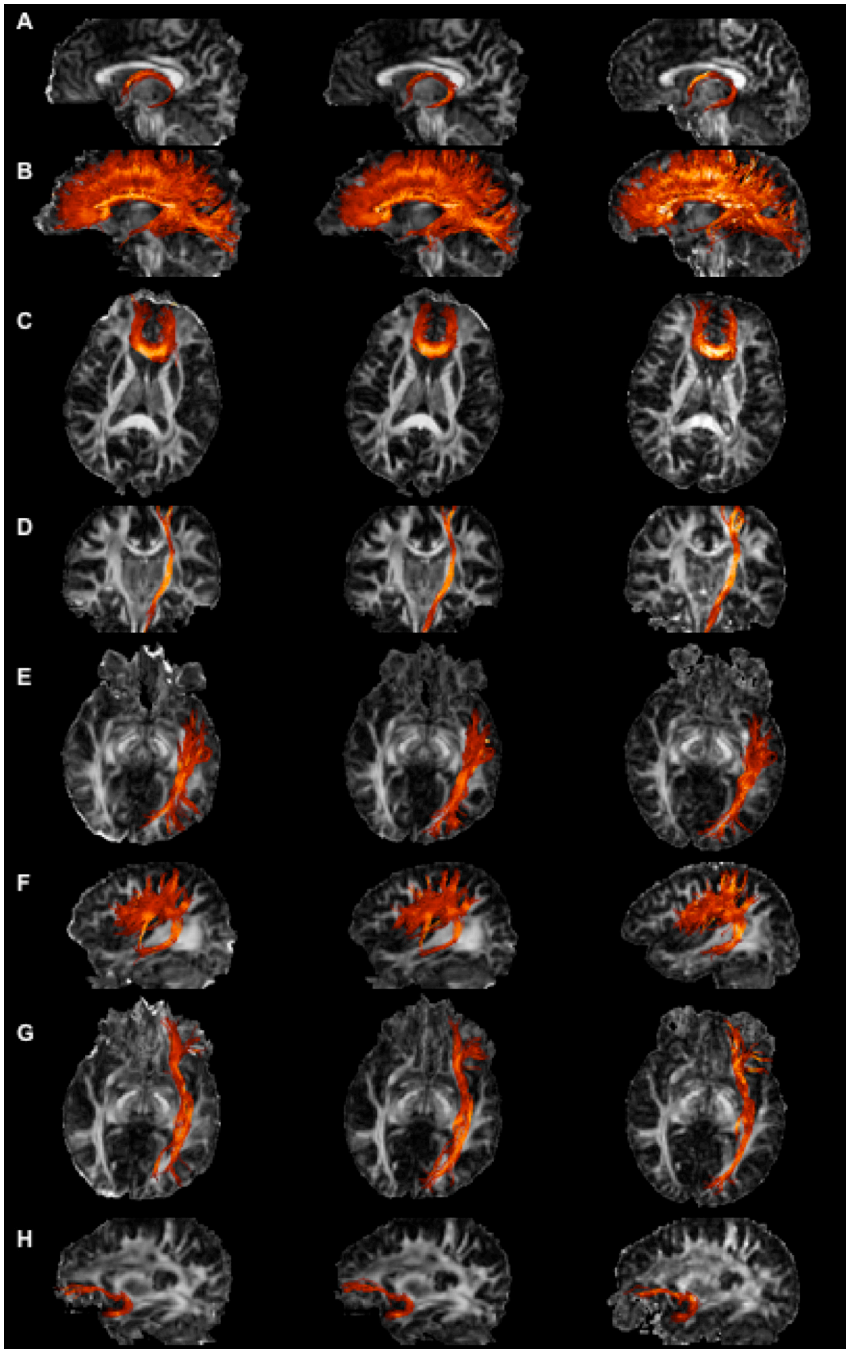

Figure 4.
Images of the fornix (A), CC (B), FM (C), CST (D), ILF (E), SLF (F), IOF (G), UF (H), produced using SE-EPI-DTI$_{12}$ (first column), SE-EPI-DTI$_{138}$ (second column), and Turboprop-DTI (third column) datasets. FA maps from the corresponding datasets are displayed in the background. The projection of all fibers assigned to a bundle is shown, independent of if the fibers are in front or behind the 2D plane of the background FA map. Bright colors correspond to fibers with high FA values and dark colors to fibers with low FA values. All data were acquired in the same scan session and on the same normal subject.

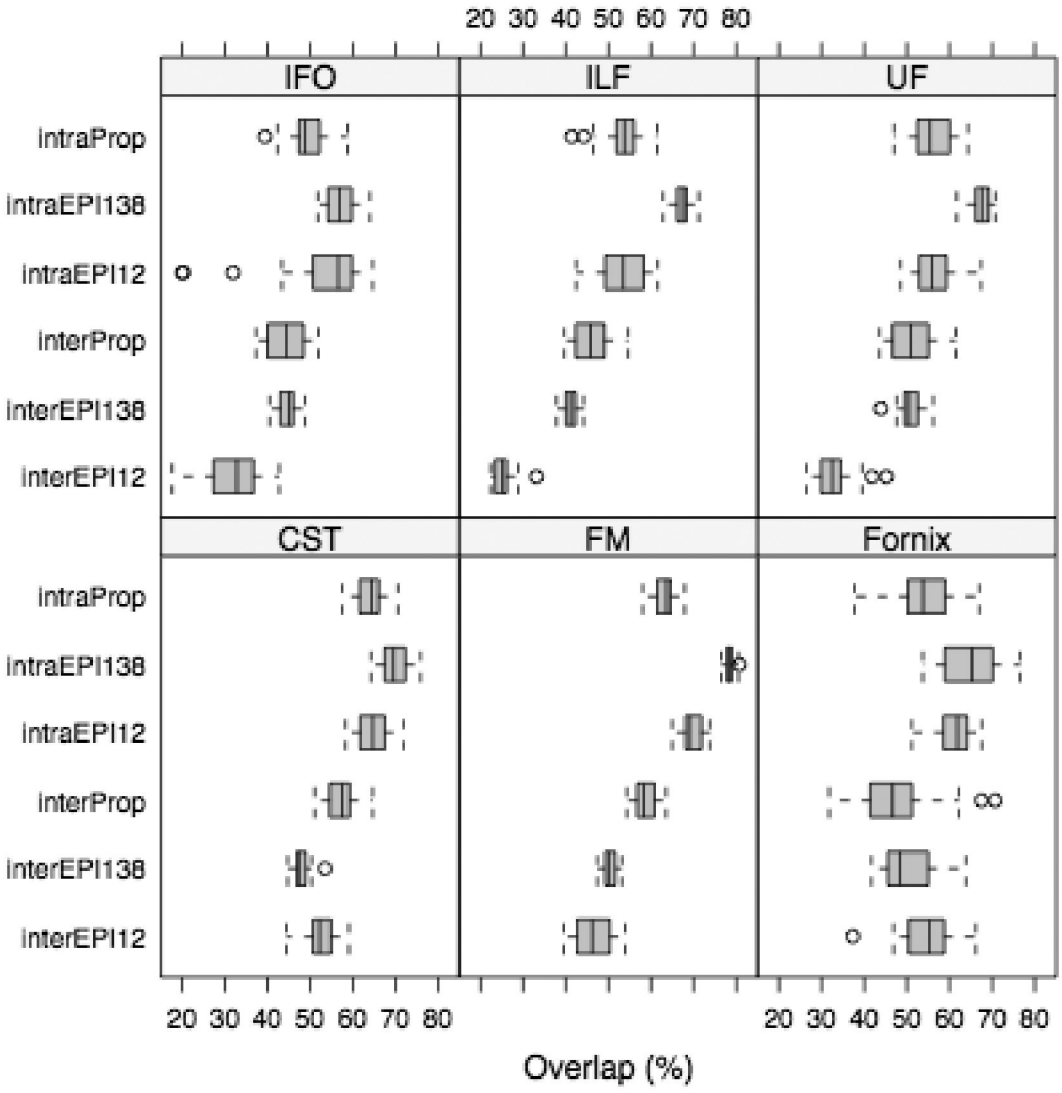

Figure 5.
Boxplots of the intra-session and inter-session reproducibility for the fibers of the UF, FM, fornix, CST, IFO, ILF, produced from SE-EPI-DTI$_{12}$, SE-EPI-DTI$_{138}$, and Turboprop-DTI datasets of subject 1.

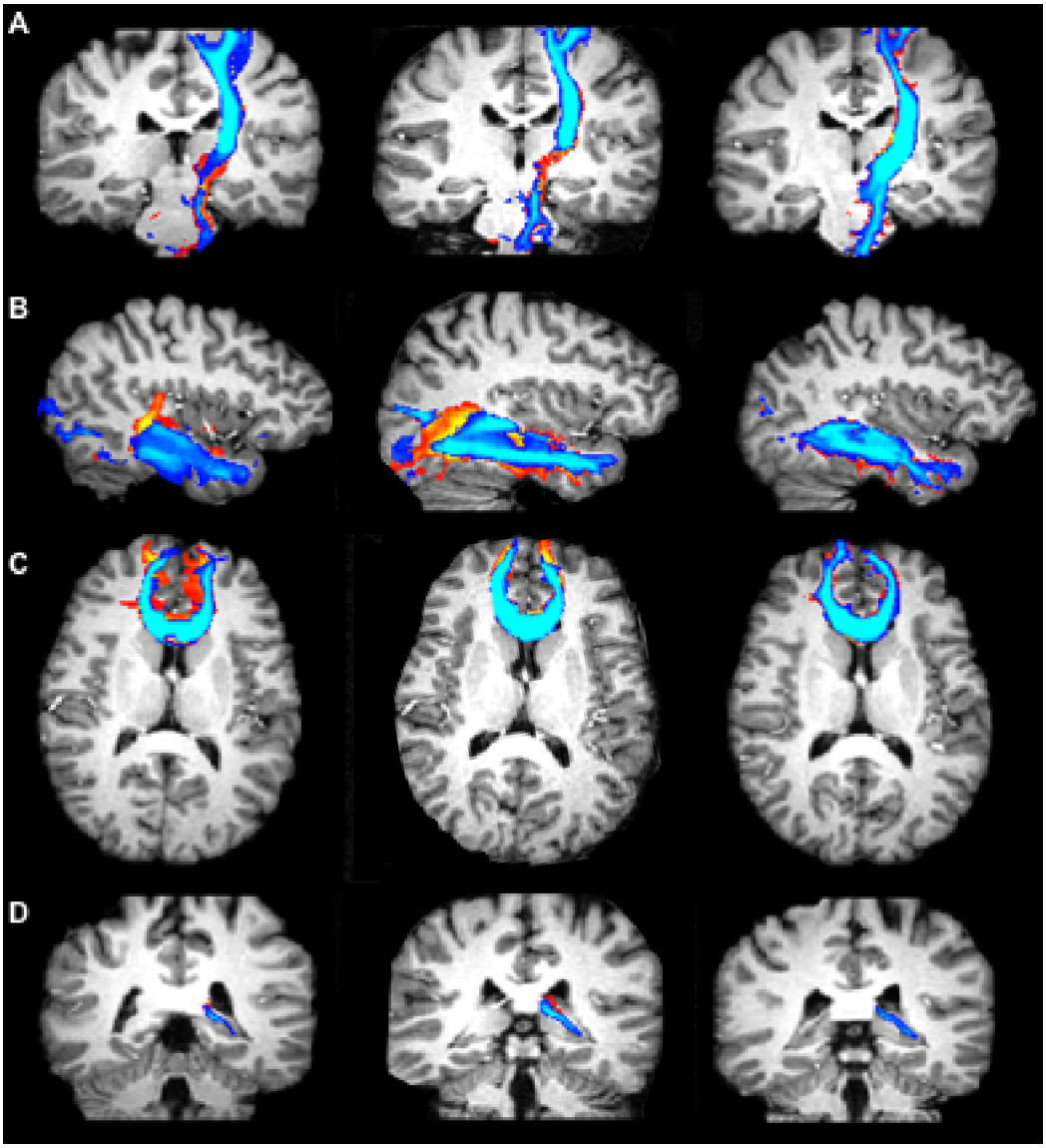

Figure 6.

Images of the cross-section of all copies of the CST (A), ILF (B), FM (C), fornix (D), produced with wild bootstrap for two separate scan sessions, with various slices of a healthy human brain. The fiber tracts were produced from data acquired with SE-EPI-DTI$_{12}$ (first column), SE-EPI-DTI$_{138}$ (second column), and Turboprop-DTI (third column). MPRAGE images from the corresponding slices are displayed in the background. Blue fibers were generated from DTI data acquired in a different position of the head than red/yellow fibers. The overlap of fibers generated from data acquired in different scan sessions is higher for Turboprop-DTI than SE-EPI-DTI$_{12}$, and SE-EPI-DTI$_{138}$.

Table 1

Intra-session reproducibility and the p-values for the comparison of intra-session reproducibility between the three types of DTI data acquisitions for subject 1.

Intra-session reproducibility (mean percentage)	Turboprop-DTI	SE-EPI-DTI$_{12}$	SE-EPI-DTI$_{138}$	P-values		
				Tp *vs.* EPI$_{12}$	Tp *vs.* EPI$_{138}$	EPI$_{12}$*vs.* EPI$_{138}$
CST	64.0%	64.8%	69.9%	0.532	0.001	0.142
IFO	49.4%	52.1%	56.9%	0.358	<0.0001	<0.0001
ILF	53.3%	53.7%	67.1%	0.835	<0.0001	<0.0001
UF	55.8%	56.3%	67.1%	0.790	<0.0001	<0.0001
FM	63.2%	69.7%	78.4%	<0.0001	<0.0001	<0.0001
Fornix	53.9%	61.0%	64.8%	0.0022	0.0005	0.301

Tp, Turboprop-DTI; EPI$_{12}$, SE-EPI-DTI$_{12}$; EPI$_{138}$, SE-EPI-DTI$_{138}$.

Table 2

Intra-session reproducibility and the p-values for the comparison of intra-session reproducibility between the three types of DTI data acquisitions for subject 2.

Intra-session reproducibility (mean percentage)	Turboprop-DTI	SE-EPI-DTI$_{12}$	SE-EPI-DTI$_{138}$	P-values		
				Tp *vs.* EPI$_{12}$	Tp *vs.* EPI$_{138}$	EPI$_{12}$*vs.* EPI$_{138}$
CST	77.9%	78.5%	80.1%	0.608	0.321	0.330
IFO	69.2%	71.9%	78.3%	0.278	0.0012	0.002
ILF	72.9%	70.3%	77.4%	0.339	0.026	0.002
UF	76.1%	75.0%	82.7%	0.689	0.004	0.003
FM	74.0%	76.0%	78.1%	0.237	0.013	0.111
Fornix	66.1%	69.0%	73.4%	0.346	0.004	0.063

Tp, Turboprop-DTI; EPI$_{12}$, SE-EPI-DTI$_{12}$; EPI$_{138}$, SE-EPI-DTI$_{138}$.

Table 3

Intra-session reproducibility and the p-values for the comparison of intra-session reproducibility between the three types of DTI data acquisitions for subject 3.

Intra-session reproducibility (mean percentage)	Turboprop-DTI	SE-EPI-DTI$_{12}$	SE-EPI-DTI$_{138}$	P-values		
				Tp *vs.* EPI$_{12}$	Tp *vs.* EPI$_{138}$	EPI$_{12}$*vs.* EPI$_{138}$
CST	73.9%	74.1%	78.5%	0.803	0.005	0.006
IFO	61.9%	63.8%	69.9%	0.504	0.001	0.001
ILF	65.2%	62.4%	68.3%	0.283	0.195	0.025
UF	68.5%	66.0%	69.6%	0.001	0.180	0.205
FM	78.9%	80.2%	78.5%	0.369	0.793	0.141
Fornix	72.0%	70.9%	75.9%	0.569	0.289	0.081

Tp, Turboprop-DTI; EPI$_{12}$, SE-EPI-DTI$_{12}$; EPI$_{138}$, SE-EPI-DTI$_{138}$.

Table 4

Intra-session reproducibility and the p-values for the comparison of intra-session reproducibility between the three types of DTI data acquisitions for subject 1.

Intra-session reproducibility (mean percentage)	Turboprop-DTI	SE-EPI-DTI$_{12}$	SE-EPI-DTI$_{138}$	P-values		
				Tp vs. EPI$_{12}$	Tp vs. EPI$_{138}$	EPI$_{12}$ vs. EPI$_{138}$
CST	57.2%	52.2%	47.8%	0.006	<0.0001	0.001
IFO	44.7%	31.9%	44.8%	<0.0001	0.92	<0.0001
ILF	45.9%	26.3%	41.1%	<0.0001	0.008	<0.0001
UF	50.9%	32.9%	50.8%	<0.0001	0.994	<0.0001
FM	58.7%	46.7%	50.3%	<0.0001	0.003	0.02
fornix	48.1%	54.4%	50.3%	0.032	0.423	0.042

Tp, Turboprop-DTI; EPI$_{12}$, SE-EPI-DTI$_{12}$; EPI$_{138}$, SE-EPI-DTI$_{138}$.

Table 5

Intra-session reproducibility and the p-values for the comparison of intra-session reproducibility between the three types of DTI data acquisitions for subject 2.

Intra-session reproducibility (mean percentage)	Turboprop-DTI	SE-EPI-DTI$_{12}$	SE-EPI-DTI$_{138}$	P-values		
				Tp vs. EPI$_{12}$	Tp vs. EPI$_{138}$	EPI$_{12}$ vs. EPI$_{138}$
CST	66.4%	62.1%	63.6%	0.038	0.12	0.268
IFO	57.6%	62.5%	67.3%	0.157	0.017	0.219
ILF	59.6%	48.3%	52.4%	0.005	0.0019	0.350
UF	63.0%	55.1%	60.1%	0.013	0.191	0.199
FM	68.7%	56.1%	62.2%	<0.0001	<0.0001	0.018
fornix	50.8%	45.8%	65.3%	0.311	<0.0001	<0.0001

Tp, Turboprop-DTI; EPI$_{12}$, SE-EPI-DTI$_{12}$; EPI$_{138}$, SE-EPI-DTI$_{138}$.

Table 6

Intra-session reproducibility and the p-values for the comparison of intra-session reproducibility between the three types of DTI data acquisitions for subject 3.

Intra-session reproducibility (mean percentage)	Turboprop-DTI	SE-EPI-DTI$_{12}$	SE-EPI-DTI$_{138}$	P-values		
				Tp vs. EPI$_{12}$	Tp vs. EPI$_{138}$	EPI$_{12}$ vs. EPI$_{138}$
CST	65.2%	60.4%	61.6%	0.0005	0.005	0.258
IFO	55.6%	56.8%	63.4%	0.430	0.061	0.053
ILF	60.5%	51.1%	55.6%	<0.0001	0.012	0.038
UF	62.7%	56.0%	60.0%	0.043	0.593	0.421
FM	74.9%	67.8%	70.8%	0.011	0.053	0.132
fornix	67.5%	63.9%	71.1%	0.386	0.413	0.050

Tp, Turboprop-DTI; EPI$_{12}$, SE-EPI-DTI$_{12}$; EPI$_{138}$, SE-EPI-DTI$_{138}$.